Modeling the Response of Electromagnetic Induction Sensors to Inhomogeneous Magnetic Soils with Arbitrary Relief

Pascal Druyts, Yogadhish Das, *Fellow, IEEE*, Christophe Craeye, *Member, IEEE* and Marc Acheroy, *Member, IEEE*

***Abstract*—A general model to compute the response of an Electromagnetic Induction (EMI) sensor to a magnetic soil, in both time and frequency domains, is developed. The model requires modest computational resources and can be applied to arbitrary soil inhomogeneities and relief, and to arbitrary sensor coil shapes, orientations and positions. Central to the model is the concept of a head sensitivity map which can be used to characterize the sensor head as a function of the shape, size and position of the sensor coils. Two further concepts related to the head sensitivity are presented, the zero equi-sensitivity surface and the volume of influence. We demonstrate that these concepts aid understanding of the detector behavior. The general model is based on the Born approximation, which is valid if the soil magnetic susceptibility is sufficiently small. A simpler model which is only valid for homogeneous Half-Space (HS) soils but does not require the Born approximation is also developed. The responses predicted by both models are shown to be in good agreement with each other and also with available analytic solutions. Comparing the two models also enabled an expression for the error incurred when using the Born approximation to be established. We shown that, for most soils of relevance to mine clearance, the corresponding error is negligible.**

***Index Terms*—Born approximation, electromagnetic induction (EMI), humanitarian demining, magnetic susceptibility, metal detector (MD), reciprocity, sensitivity map.**

I. Introduction

METAL Detectors (MDs) working on the principle of EMI are widely used in mine action. Many factors must be taken into account to understand the performance of a MD including the detector characteristics, the target response, the soil response and the effect of the soil on the target response. Detector characteristics include factors such as internal processing, geometry of the detector head and transmit current. Many authors [1]–[8] have proposed methods to assess the target response but the influence of the soil has received less attention until recently. Nevertheless it was known that the soil can significantly affect metal detectors and, as a result, manufacturers provide most high-end MDs with soil compensation capabilities. Unfortunately, due to competition among manufacturers, details of the soil compensation techniques implemented are often proprietry, although some information is available in patents [9].

The soil can effect the target response and it can provide an additional contribution to the detector response [10]–[14]. Here we concentrate on the response of the soil in the absence of target. This response is of prime importance as it can be the source of false alarms or require the use of a lower detector sensitivity setting which in turn will reduce the target detectability.

The soil response is influenced by many factors such as the current waveform in the Transmit (TX) coil, the detector head geometry, the coil electrical characteristics, the detector electronics and the soil electromagnetic properties. Some of these factors have been studied [12], [14]–[18], but many open questions still remain. For example, in many cases analytic models have been used and, as a result, the analysis was restricted to simple coil arrangements such as concentric circular coils, and to homogeneous soils with a flat air-soil interface. However, the shape and relative position of the coils have a major impact on detector performance which is indicated by the amount of different coil arrangements used in practice [19]. The soil relief and soil inhomogeneities also have a major impact on detector performance.

We show that the soil response can be expressed for general head geometries and for general soil inhomogeneities and reliefs by resorting to a general form of reciprocity and we directly derive that reciprocity expression for the Magneto-Quasi-Static (MQS) regime relevant to MDs. The resulting expression for the soil response includes the magnetic field produced by the TX coil in the presence of soil. Computing that field for a general soil and for a general head geometry requires the use of computationally intensive numerical methods.

However, several publications [12], [17] suggest that for most soils of interest the response is mainly due to the soil magnetic susceptibility and therefore effects of soil conductivity may be neglected. Furthermore, the magnetic susceptibilities of most natural soils are quite low [20]–[26].

In this paper we show that for such soils, with negligible electric conductivity and low magnetic susceptibility, major simplifications can be achieved by using the Born approximation. This also allows more realistic scenarios to

This work was supported by the Belgian Defence.

P. Druyts and M. Acheroy are with the Royal Military Academy, Signal and Image Centre, Av. de la Renaissance 30, B-1000 Brussels, Belgium (e-mail: Pascal.Druyts@elec.rma.ac.be).

Y. Das is with Defence R&D Canada – Suffield, Alberta, Canada.

C. Craeye is with Université Catholique de Louvain, Electrical Engineering department, Place du Levant 3, B-1348 Louvain-la-Neuve, Belgium.

be studied efficiently and the effects of head geometry, soil inhomogeneity and relief on MD performance to be taken into account.

In addition to this general model, a second model based on image theory is developed. That model is only valid for a homogeneous HS but it does not require the Born approximation. It is therefore also valid for soils with high magnetic susceptibilities. The responses predicted by both models are compared with each other and also with available analytical solutions. The comparison shows good agreement between the results and this provides a means of validation for the models and their implementations. Comparing the two models also allows us to establish an expression for the error incurred when using the Born approximation. In the light of susceptibility measurements of many soils found in the literature it can be demonstrated that, for most soils of interest to mine clearance, the corresponding error is negligible.

The models are developed in the frequency domain. It is then shown that, under reasonable assumptions, the results can efficiently be extended to the time domain.

The paper is organized as follows. Section II describes the problem and Section III presents the notation and conventions used. Both models to compute the soil response in the frequency domain are presented in Section IV-A. The first is valid for arbitrary soil inhomogeneity and relief but relies on the Born approximation whereas the second is only valid for homogeneous HS configurations but does not require the Born approximation. Section IV-A4 compares both models in order to assess the accuracy of the Born approximation. Section IV-B extends the models to apply to the time domain which is better suited to analyze pulse induction detectors. Section V presents some simple applications of the models, including the zero equi-sensitivity surface and the volume of influence. Finally Section VI concludes the paper and gives some perspectives for more practical use of the proposed general model.

II. Problem description

The problem considered is sketched in Fig. 1 (a). A MD head is located at an arbitrary position and with an arbitrary orientation above the soil. The head is in general composed of a TX and a Receive (RX) coil, but a single coil can also be used for both reception and transmission.

The soil is assumed to be non-conductive and has a magnetic susceptibility varying both with frequency and position. The magnetic susceptibility is denoted $\chi(\omega,\boldsymbol{r})$, with ω the angular frequency and $\boldsymbol{r}$ the position vector.

Consideration of magnetic susceptibility that varies spatially allows us to take into account soils with arbitrary inhomogeneity and relief. In addition, we consider a magnetic susceptibility that varies with frequency because some naturally occurring soils exhibit such behavior [24], [26] and it has been shown [12], [17] that this frequency variation (also known as viscous remanent magnetization, magnetic viscosity, magnetic relaxation or magnetic after-effect) has a significant effect on MDs.

The model can be used for an arbitrary head configuration and fig. 2 presents commonly used [19] head configurations which will be considered in this paper.

The coil overlap for the double-D head is chosen to obtain zero coupling between the coils in the absence of soil. The quad coil is composed of two RX half-circles connected in opposition (i.e., the current flows in opposite directions in the two circular segments and in the same direction in the two straight segments).

III. Conventions and notations

Vectors and scalars are denoted $\boldsymbol{x}$ and x respectively. $\|\boldsymbol{x}\|$ is the magnitude of $\boldsymbol{x}$ and $\hat{\boldsymbol{x}} = \frac{\boldsymbol{x}}{\|\boldsymbol{x}\|}$ is a unit vector. Volumes, surfaces and contours are denoted $\mathcal{V}_{\mathrm{x}}$, $\mathcal{S}_{\mathrm{x}}$ and $\mathcal{C}_{\mathrm{x}}$ respectively. $\mathcal{V}_\infty$ is the whole space which is bounded by the infinite sphere $\mathcal{S}_\infty$.

The volume, surface and contour elements are denoted by $\mathrm{d}V$, $\mathrm{d}S$ and $\mathrm{d}l$ respectively and $\mathrm{d}\boldsymbol{S} = \hat{\boldsymbol{n}}\mathrm{d}S$ and $\mathrm{d}\boldsymbol{l} = \hat{\boldsymbol{l}}\mathrm{d}l$ are the corresponding vector quantities where the unit positive normal and tangent are $\hat{\boldsymbol{n}}$ and $\hat{\boldsymbol{l}}$ respectively.

The subscript 'x' is a label which identifies the volume, surface or contour. When the same label is used for a volume $\mathcal{V}_{\mathrm{x}}$ and a surface $\mathcal{S}_{\mathrm{x}}$, the surface is defined as the boundary of the volume and its positive normal points outside $\mathcal{V}_{\mathrm{x}}$. When the same label is used for a (open) surface $\mathcal{S}_{\mathrm{x}}$ and a (closed) contour $\mathcal{C}_{\mathrm{x}}$, the contour is defined as the boundary of the surface whereas the positive normal of $\mathcal{S}_{\mathrm{x}}$ and the positive tangent of $\mathcal{C}_{\mathrm{x}}$ are related by the right-hand rule.

When presenting results, dimensionless quantities are used. The dimensionless quantity corresponding to the scalar x and vector $\boldsymbol{x}$ will be denoted x and $\mathbf{x}$ respectively.

Unless otherwise specified, harmonic sources and fields are considered with an $e^{j\omega t}$ time variation assumed and suppressed.

A source is identified by its label 's' and the corresponding current distribution is denoted $\boldsymbol{J}_{\mathrm{s}}$. When such a source is radiating in an environment defined as 'env' the corresponding magnetic field is denoted by $\boldsymbol{H}_{\mathrm{s}}^{(\mathrm{env})}$. A similar notation is used for the corresponding magnetic induction $\boldsymbol{B}_{\mathrm{s}}^{(\mathrm{env})}$ and magnetic vector potential $\boldsymbol{A}_{\mathrm{s}}^{(\mathrm{env})}$. When reciprocity is used, states are denoted $\Sigma_{\mathrm{s}}^{(\mathrm{env})}$ where 's' is the source and 'env' the environment characterizing these states.

IV. Development of Soil EMI Response Models

A. Soil response in the frequency domain

In this section, we describe the development of a general model valid for arbitrary soil relief and inhomogeneity. We then describe our development of a simpler model that is only applicable to HS homogeneous soils. Both models can be used for a HS configuration and comparing their results allows the accuracy of the Born approximation underlying the general model to be assessed (see Section IV-A4).

1) Assumptions: Since we are considering the case of low conductivity soils and that frequencies used in EMI detectors are less than 100kHz the MQS approximation can be used [27].

Let us consider a head composed of the ideal TX and RX coils. An ideal TX coil is comprised of a single closed-loop made of an infinitely thin wire where the current remains constant because no charge is accumulated due to parasitic

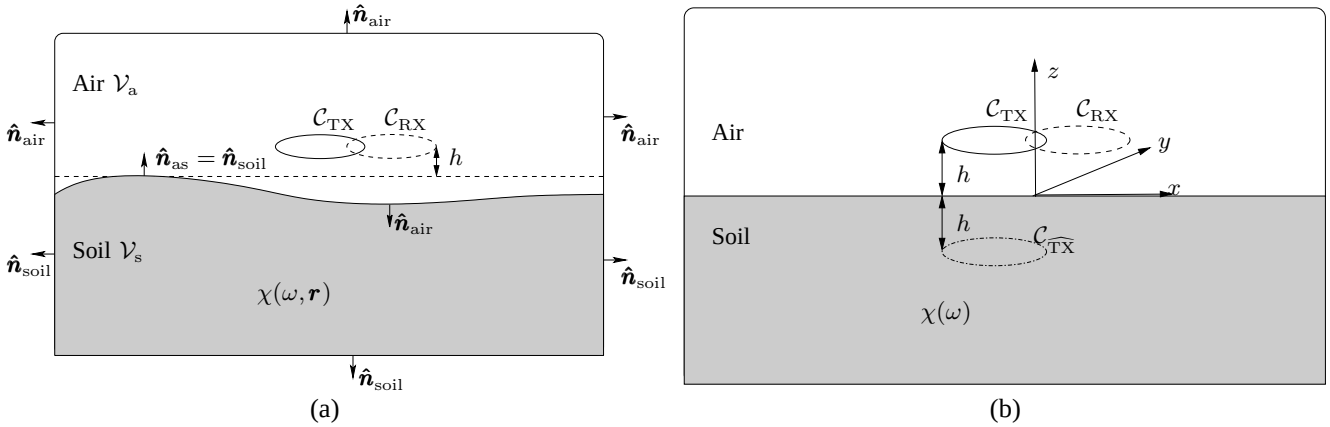

Fig. 1. MD composed of TX and RX coils ($\mathcal{C}_{\rm TX}$ and $\mathcal{C}_{\rm RX}$) of arbitrary shapes above magnetic soil. (a) general inhomogeneous soil exhibiting some relief and (b) homogeneous HS with $\mathcal{C}_{\widehat{\rm TX}}$ the mirror image of the TX coil, used to compute the soil response, and h the height of the head above the soil.

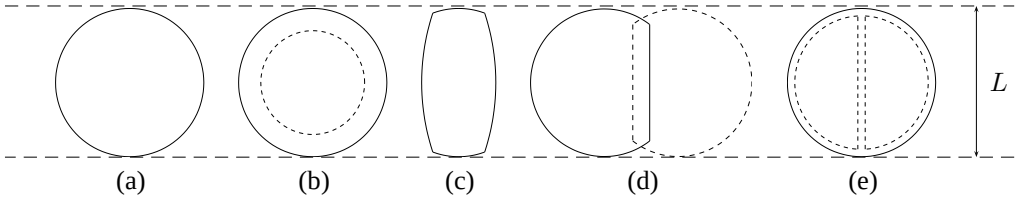

Fig. 2. Head configurations considered. TX — and RX – – coils for (a) circular, (b) concentric, (c) elliptic, (d) double-D and (e) quad heads. For circular and elliptic heads, a single coil is used for RX and TX. L is the head characteristic length.

capacitance. Under these conditions the current distribution $\boldsymbol{J}_{\rm TX}$ is fully defined by the closed curve $\mathcal{C}_{\rm TX}$ corresponding to the shape of the coil and by the current $I_{\rm TX}$ flowing through any cross section.

Similarly, an ideal RX coil is defined by the closed curve $\mathcal{C}_{\rm RX}$ and the induced voltage is equal to the derivative of the magnetic flux through a surface $\mathcal{S}_{\rm RX}$ bound by the contour $\mathcal{C}_{\rm RX}$:

$$e_{\rm RX} = j\omega \int_{\mathcal{S}_{\rm RX}} \boldsymbol{B}_{\rm TX}^{\rm (as)} \cdot {\rm d}\boldsymbol{S} = -\omega \oint_{\mathcal{C}_{\rm RX}} \boldsymbol{A}_{\rm TX}^{\rm (as)} \cdot {\rm d}\boldsymbol{l} \qquad (1)$$

Where $\boldsymbol{B}_{\rm TX}^{\rm (as)}$ and $\boldsymbol{A}_{\rm TX}^{\rm (as)}$ are the magnetic induction and the magnetic vector potential produced by the source current distribution $\boldsymbol{J}_{\rm TX}$ in the TX coil and the term '(as)' indicates that the environment is composed of air and soil.

In the case of a two-coil head, current may be induced in the RX coil. This current should be considered as part of the TX current $\boldsymbol{J}_{\rm TX}$. As a result, $\boldsymbol{J}_{\rm TX}$ should be described by two currents, one flowing on $\mathcal{C}_{\rm TX}$ and the other on $\mathcal{C}_{\rm RX}$. This generalization is straightforward and will therefore not be discussed further.

In general, the TX current when the head is in the presence of soil may be different to when it is in free space. We use the TX current in the presence of soil in equation (1) and in the rest of this paper unless explicitly stated. As this current varies with soil properties, sensor height and orientation it should be related to the free space TX current, which can be measured and considered as a detector characteristic. For most cases this distinction is not critical because the soil response is small and will not significantly change the TX current. The TX current in the presence of soil is further discussed in Appendix A.

2) General model: The voltage induced in the RX coil (1) includes the following two contributions:

- $e_{\rm RX}^{\rm TX}$ resulting from the direct coupling between TX and RX coils
- $e_{\rm RX}^{\rm soil} \triangleq e_{\rm RX} - e_{\rm RX}^{\rm TX}$ resulting from the soil response

The direct coupling is often of little interest because it remains constant[1] and it is canceled by the detector electronics. If required, it can be calculated using an expression similar to (1):

$$e_{\rm RX}^{\rm TX} = j\omega \oint_{\mathcal{C}_{\rm RX}} \boldsymbol{A}_{\rm TX}^{\rm (fs)} \cdot {\rm d}\boldsymbol{l} \qquad (2)$$

where '(fs)' indicates the free space environment. It can also be expressed as $e_{\rm RX}^{\rm TX} = j\omega M_{\rm TX,RX} I_{\rm TX}$ where the mutual induction coefficient $M_{\rm TX,RX}$ between the TX and RX coils can be measured directly. For single coil detectors, the direct coupling becomes $e_{\rm RX}^{\rm TX} = j\omega L_{\rm TX} I_{\rm TX}$ where $L_{\rm TX}$ is the TX coil self-induction coefficient. For the single coil case, (2) can no longer be used because $A_{\rm TX}^{\rm (fs)}$ becomes infinite on the coil. This singularity is due to the filament assumption and disappears if the current distribution across the coil conductor is taken into account. Nevertheless, measuring $L_{\rm TX}$ is straightforward.

We define the voltage $e_{\rm RX}^{\rm soil}$ induced in the RX coil by the soil as the *soil response*. To simplify the notation, it will be denoted $V_{\rm soil}$ given by:

$$V_{\rm soil} = j\omega \int_{\mathcal{C}_{\rm RX}} \boldsymbol{A}_{\rm soil}^{\rm (fs)} \cdot {\rm d}\boldsymbol{l} \qquad (3)$$

[1]Assuming that the soil does not significantly change $I_{\rm TX}$ (see Appendix A)

with $\boldsymbol{A}_{\rm soil}^{\rm (fs)} = \boldsymbol{A}_{\rm TX}^{\rm (as)} - \boldsymbol{A}_{\rm TX}^{\rm (fs)}$ which can be interpreted as the magnetic vector potential produced by equivalent currents[2] $\boldsymbol{J}_{\rm soil}$ in the soil volume. Indeed the soil, like any other medium, can be substituted by equivalent currents flowing in free space [28], [29]. It should be noted that $\boldsymbol{A}_{\rm soil}^{\rm (fs)}$ is always finite, making (3) valid for single coil detectors.

Equation (3) is computationally inefficient because of the requirement to calculate the equivalent currents, use the equivalent current distribution to calculate, by means of an integration on the soil volume, the vector potential $\boldsymbol{A}_{\rm soil}^{\rm (fs)}$ on the RX where a line integration must be performed..

A more practical expression can be obtained by the use of reciprocity to relate fields in two configurations (called states). Various reciprocity relations can be found in the literature [28]–[30] but the most generic expression, which takes into account different media in both states, is seldom used [31], [32]. The MQS expressions used in this paper could be obtained by introducing[3] the MQS approximations in [32, Equ. 3]. Alternatively, Appendix B presents a direct derivation of the general MQS reciprocity relation.

Applying reciprocity (Equ. B.3 of Appendix B) over $\mathcal{V}_\infty$ (the whole space) with the two following states:

- $\Sigma_{\rm TX}^{\rm (as)}$ which is the state for which the current $I_{\rm TX}$ flows in the TX coil in presence of soil
- $\Sigma_{\rm RX}^{\rm (fs)}$ which is the state for which the current $I_{\rm RX}$ flows[4] in the RX coil in absence of soil

yields:

$$\int_{\mathcal{S}_\infty} \left(\boldsymbol{A}_{\rm TX}^{\rm (as)} \times \boldsymbol{H}_{\rm RX}^{\rm (fs)} - \boldsymbol{A}_{\rm RX}^{\rm (fs)} \times \boldsymbol{H}_{\rm TX}^{\rm (as)}\right) \cdot {\rm d}\boldsymbol{S} = \int_{\mathcal{V}_\infty} \Big\{(\mu_{\rm TX} - \mu_{\rm RX})\boldsymbol{H}_{\rm TX}^{\rm (as)} \cdot \boldsymbol{H}_{\rm RX}^{\rm (fs)} + \boldsymbol{J}_{\rm TX} \cdot \boldsymbol{A}_{\rm RX}^{\rm (fs)} - \boldsymbol{J}_{\rm RX} \cdot \boldsymbol{A}_{\rm TX}^{\rm (as)}\Big\} {\rm d}V \quad (4)$$

where $\mu_{\rm TX}$ and $\mu_{\rm RX}$ are the magnetic permeabilities for states $\Sigma_{\rm TX}^{\rm (as)}$ and $\Sigma_{\rm RX}^{\rm (fs)}$ respectively.

The contrast $\mu_{\rm TX} - \mu_{\rm RX}$ is zero except in the soil volume $\mathcal{V}_{\rm s}$ (see Fig. 1) where it is equal to $\mu_0\chi$ where χ is the magnetic susceptibility of the soil. The contribution of the sources to the volume integral reduces to the sum of two contour integrals, one on $\mathcal{C}_{\rm TX}$ and the other on $\mathcal{C}_{\rm RX}$ because the sources are concentrated on those contours. By considering that the integral on the infinite sphere $\mathcal{S}_\infty$ vanishes according to the far field behavior of fields and potentials, simplifying (4) to:

$$\mu_0 \int_{\mathcal{V}_{\rm s}} \chi \boldsymbol{H}_{\rm TX}^{\rm (as)} \cdot \boldsymbol{H}_{\rm RX}^{\rm (fs)} {\rm d}V = I_{\rm RX} \oint_{\mathcal{C}_{\rm RX}} \boldsymbol{A}_{\rm soil}^{\rm (fs)} \cdot {\rm d}\boldsymbol{l} \quad (5)$$

where the contour integral on $\mathcal{C}_{\rm TX}$ was replaced according to:

$$I_{\rm RX} \oint_{\mathcal{C}_{\rm RX}} \boldsymbol{A}_{\rm TX}^{\rm (fs)} \cdot {\rm d}\boldsymbol{l} = I_{\rm TX} \oint_{\mathcal{C}_{\rm TX}} \boldsymbol{A}_{\rm RX}^{\rm (fs)} \cdot {\rm d}\boldsymbol{l} \quad (6)$$

[2]These currents do not exist physically because the soil was assumed non-conductive.

[3]Replace $\boldsymbol{E}$ by $-j\omega\boldsymbol{A}$, note that there is no electric charge and no magnetic current in this case and take the limit as $\omega \to 0$.

[4]As already mentioned, current may be induced in the RX coil by the TX current. This induced current should not be confused with $I_{\rm RX}$ which is a fictitious current used to apply reciprocity.

which is obtained easily by applying reciprocity over the whole space, while considering the states $\Sigma_{\rm TX}^{\rm (fs)}$ and $\Sigma_{\rm RX}^{\rm (fs)}$ defined as above, but with the free space environment for both states.

With (5), (3) becomes:

$$V_{\rm soil} = j\omega\mu_0 I_{\rm TX} \int_{\mathcal{V}_{\rm s}} \chi \check{\boldsymbol{H}}_{\rm TX}^{\rm (as)} \cdot \check{\boldsymbol{H}}_{\rm RX}^{\rm (fs)} {\rm d}V \quad (7)$$

with $\check{\boldsymbol{H}}_{\rm coil}^{\rm (env)} = \boldsymbol{H}_{\rm coil}^{\rm (env)}/I_{\rm coil}$ the magnetic field normalized with respect to the corresponding coil current[5]. Similar expressions have been obtained in the framework of nondestructive testing. For example, in [33, Equ. 16b] Auld *et al.* present an expression for the impedance variation $\triangle Z_{12}$ related to the soil response by $V_{\rm soil} = \triangle Z_{12} I_{\rm TX}$. Both expressions were obtained following different lines of reasoning and are identical under the MQS approximation, since the electric term appearing in [33, Equ. 16b] is then zero.

Recalling that the voltage induced in the RX coil by a magnetic dipole $\boldsymbol{m}$ is [34, Equ. 2.21 p. 23]:

$$V_{\rm dip} = j\omega\mu_0 \boldsymbol{m} \cdot \check{\boldsymbol{H}}_{\rm RX}^{\rm (fs)} \quad (8)$$

equation (7) can be physically interpreted as the sum of contributions by elementary magnetic dipoles:

$${\rm d}\boldsymbol{m} = \chi I_{\rm TX} \check{\boldsymbol{H}}_{\rm TX}^{\rm (as)} {\rm d}V \quad (9)$$

The computation of $\boldsymbol{H}_{\rm TX}^{\rm (as)}$ for a general soil usually requires numerical techniques which are computationally intensive. However, for low susceptibilities, $\boldsymbol{H}_{\rm TX}^{\rm (as)}$ can be approximated accurately by $\boldsymbol{H}_{\rm TX}^{\rm (fs)}$, which is easier to compute. This is the Born approximation [35, Equ. 8.10.1 p. 485] [33, Section 2.3.1.2]. In [36] the Born approximation is also used in the scope of landmine detection to compute the response of a dielectric mine. The accuracy of the Born approximation can be evaluated for simple configurations, such as a homogeneous HS, for which analytic solutions exist. This approximation is further discussed in Section IV-A4 and it is shown to be quite accurate for most soils of interest.

Replacing $\check{\boldsymbol{H}}_{\rm TX}^{\rm (as)}$ by $\check{\boldsymbol{H}}_{\rm TX}^{\rm (fs)}$ in (7) yields for the soil response:

$$V_{\rm soil} = j\omega\mu_0 I_{\rm TX} \int_{\mathcal{V}_{\rm s}} \chi S {\rm d}V \quad (10)$$

where

$$S = \check{\boldsymbol{H}}_{\rm TX}^{\rm (fs)} \cdot \check{\boldsymbol{H}}_{\rm RX}^{\rm (fs)} \quad (11)$$

is defined as the sensitivity of the head. The concept of sensitivity map was first introduced in [37] to characterize the response of a MD to a small sphere. According to (10), it is also useful to compute the soil response. In [37], sensitivity maps were computed for rectangular coil arrangements. In Section V-A we present results for more complex heads.

In (11), only free space magnetic fields appear; for an arbitrary coil geometry $\mathcal{C}_{\rm coil}$, they can be computed by means of the Biot-Savart law [29, Equ. 13 p. 230 and Equ. 11 p. 232]:

$$\check{\boldsymbol{H}}_{\rm coil}^{\rm (fs)}(\boldsymbol{r}) = \frac{1}{4\pi} \int_{\mathcal{C}_{\rm coil}} \frac{\hat{\boldsymbol{l}}' \times \boldsymbol{R}}{R^3} {\rm d}l' \quad (12)$$

[5]The units of $\boldsymbol{H}$ and $\check{\boldsymbol{H}}$ are respectively [A/m] and [1/m].

where $\mathcal{C}_{\rm coil}$ is the contour representing the coil, $\boldsymbol{r}$ a field point, $\boldsymbol{r}'$ a source point, $\boldsymbol{R} = \boldsymbol{r} - \boldsymbol{r}'$ is the vector joining a source point to a field point, $R = \|\boldsymbol{R}\|$ is the magnitude of $\boldsymbol{R}$ and $\hat{\boldsymbol{l}}'$ is the unit tangent to $\mathcal{C}_{\rm coil}$ at $\boldsymbol{r}'$. The coils considered in this paper (see Fig. 2) and most coils used in practice are composed of circles, circular arcs and line segments. For such coils, the magnetic $\check{\boldsymbol{H}}^{(\rm fs)}_{\rm coil}$ can be computed analytically [38]. This is a quite significant advantage because the magnetic fields must be computed for a large number of points to accurately compute (10).

3) HS model: Analytic solutions for concentric circular coils above a homogeneous HS are well known [10]. In general, they require the computation of Sommerfeld integrals. Simpler solutions may be used under the MQS approximation. They can be obtained from the general solution as in [11]. In this section, we show that the same expression as in [11] can be obtained directly by using the image theory. Furthermore, this approach provides a better physical interpretation of the results and can be generalized to arbitrary head configurations.

The image theory is often presented [29] as a method to solve electro-static problems. Nevertheless, it is easily transposed to the MQS framework.

The configuration considered is sketched in Fig. 1 (b). The field in the upper HS is the sum of the field produced by the TX coil in absence of soil and the field scattered by the soil. According to image theory, the soil contribution is assumed equal to the field produced by a fictitious current $\alpha_{\rm s} I_{\rm TX}$ flowing through the image coil $\mathcal{C}_{\widehat{\rm TX}}$, this current being the mirror image of the TX coil through the air-soil interface and radiating in free space:

$$\boldsymbol{H}^{(\rm as)}_{\rm TX}(\boldsymbol{r}_{\rm air}) = I_{\rm TX}\check{\boldsymbol{H}}^{(\rm fs)}_{\rm TX} + \alpha_{\rm s} I_{\rm TX}\check{\boldsymbol{H}}^{(\rm fs)}_{\widehat{\rm TX}} \tag{13}$$

where the argument $\boldsymbol{r}_{\rm air}$ has been introduced to emphasize the fact that the expression is only valid in the upper HS. Similarly, we assume that the field in the lower HS is equal to the one produced by a current $\alpha_{\rm t} I_{\rm TX}$ flowing in the TX coil $\mathcal{C}_{\rm TX}$ and radiating in infinite soil:

$$\boldsymbol{H}^{(\rm as)}_{\rm TX}(\boldsymbol{r}_{\rm soil}) = \alpha_{\rm t} I_{\rm TX}\check{\boldsymbol{H}}^{(\rm fs)}_{\rm TX} \tag{14}$$

where the argument $\boldsymbol{r}_{\rm soil}$ denotes that the expression is only valid in the lower HS. We replaced the normalized magnetic field $\check{\boldsymbol{H}}^{(\rm soil)}_{\rm TX}$ produced by the TX current in an infinite space filled with soil by $\check{\boldsymbol{H}}^{(\rm fs)}_{\rm TX}$, since both quantities are equal. The fields appearing in (13) and (14) can be computed easily by means of the Biot-Savart law (12) because all equivalent currents are radiating in free space.

The coefficients are solved for by applying interface conditions (continuity of the tangential component of $\boldsymbol{H}$) and by resorting to the symmetry relations (C.2). This yields:

$$\alpha_{\rm t} = \frac{2\mu_0}{\mu_0 + \mu_{\rm s}} = \frac{2}{2+\chi} \tag{15a}$$

$$\alpha_{\rm s} = \frac{\mu_{\rm s} - \mu_0}{\mu_{\rm s} + \mu_0} = \frac{\chi}{2+\chi} \tag{15b}$$

with $\mu_{\rm s} = \mu_0(1+\chi)$ the soil magnetic permeability.

In Section IV-A2, the soil response is defined as the additional voltage induced by the field scattered by the soil. Therefore, according to (13), it is equal to the voltage induced in the RX coil by a current $\alpha_{\rm s} I_{\rm TX}$ flowing through the mirrored TX coil, both coils being in free space. This voltage can be expressed as:

$$V_{\rm HS} = j\omega\alpha_{\rm s} I_{\rm TX} M_{\widehat{\rm TX},\rm RX} \tag{16}$$

where $M_{\widehat{\rm TX},\rm RX}$, the mutual induction coefficient between the RX coil and the mirrored TX coil, can be expressed as:

$$M_{\widehat{\rm TX},\rm RX} = \int_{\mathcal{C}_{\rm RX}} \check{\boldsymbol{A}}^{(\rm fs)}_{\widehat{\rm TX}} \cdot {\rm d}\boldsymbol{l} \tag{17}$$

where $\check{\boldsymbol{A}}^{(\rm fs)}_{\widehat{\rm TX}} = \boldsymbol{A}^{(\rm fs)}_{\widehat{\rm TX}}/I_{\rm TX}$, the magnetic vector potential produced by the mirrored TX coil and normalized by the corresponding current, is related to its source [29, Equ. 8 p. 231] by the following expression:

$$\check{\boldsymbol{A}}^{(\rm fs)}_{\widehat{\rm TX}}(\boldsymbol{r}) = \frac{\mu_0}{4\pi}\int_{\mathcal{C}_{\widehat{\rm TX}}} \frac{1}{R}{\rm d}\boldsymbol{l}' \tag{18}$$

with ${\rm d}\boldsymbol{l}'$ the unit tangent to $\mathcal{C}_{\widehat{\rm TX}}$ at the source point and R the distance between source and field points. For coils composed of circles, circular arcs and line segments, the magnetic potential $\check{\boldsymbol{A}}^{(\rm fs)}_{\widehat{\rm TX}}$ can be computed analytically [38]. In addition, for coaxial circular coils, the following analytic expression can be used to directly compute the mutual induction coefficient [29, Equ. 7 p. 263]:

$$M_{\widehat{\rm TX},\rm RX} = \mu_0\frac{2\sqrt{ab}}{k}\left[\left(1 - \frac{k^2}{2}\right)K(k) - E(k)\right] \tag{19}$$

where K, E are the complete elliptic integrals of first and second kinds, $k^2 = 4ab/[(a+b)^2 + d^2]$, with a and b the radii of the coils and d the distance between the centres. Substitution of (19) into (16) yields an expression for the soil response that is identical to [11, Equ. 10]. However, our approach is more general and can be applied to other head configurations.

4) Accuracy of the general model for HS soils: The expression for a general soil response (10) was obtained under the Born approximation, which assumes that the soil does not significantly change the TX field ($\boldsymbol{H}^{(\rm as)}_{\rm TX} \simeq \boldsymbol{H}^{(\rm fs)}_{\rm TX}$). Such an assumption was not required to develop the HS model expression (16). Since both expressions can be used for a HS soil, the comparison of the results allows us to quantify the accuracy of the general expression (10) for that specific configuration.

As shown in Appendix C, the mutual induction coefficient appearing in (16) can be expressed as a volume integral on the soil volume (C.5). Furthermore, for a homogeneous HS, the magnetic susceptibility may be moved outside the integral (10). As a consequence, both approaches yield a similar expression for a uniform HS soil:

$$V^{\rm i}_{\rm HS} = \beta_{\rm i} j\omega\mu_0 I_{\rm TX}\int_{\mathcal{V}_{\rm LHS}} S{\rm d}V \tag{20}$$

where $\mathcal{V}_{\rm LHS}$ is the lower HS volume $z < 0$, 'i = g' and 'i = HS' respectively for the general and HS model. According to (10) $\beta_{\rm g} = \chi$ while according to (16) and (C.5) $\beta_{\rm HS} = 2\chi/(2+\chi)$.

The relative error due to the Born approximation is thus:

$$|\frac{\beta_{\mathrm{HS}}-\beta_{\mathrm{g}}}{\beta_{\mathrm{HS}}}| = \frac{|\chi|}{2} \tag{21}$$

In [39], soils are classified according to their magnetic susceptibility as neutral, moderate, severe, and very severe depending on their effect on MDs used in the framework of mine clearance. Very severe soils have susceptibilities above 0.02. Many soils of interest indeed have susceptibilities below 0.02, as confirmed by many measurement campaigns [20]–[26]. A noticeable exception is Playa Gorgana in Panama, which is rich in pure magnetite and for which susceptibilities close to 1 have been measured [24]. For a very severe soil with a magnetic susceptibility of 0.02, the relative error is 0.01, which shows that the approximation is expected to be quite good for most soils of interest in the framework of mine clearance.

B. Soil response in the time domain

The time domain response can be obtained from the frequency domain response by Fourier transform. This requires one to compute the spectral representation $I^{\omega}_{\mathrm{TX}}(\omega) = \mathcal{F}\{I^{\mathrm{t}}_{\mathrm{TX}}(t)\}$ of the time domain TX current $I^{\mathrm{t}}_{\mathrm{TX}}(t)$ and to repeat the computation of the soil response (10) for a number of frequencies within the detector bandwidth.

The soil magnetic susceptibility is mainly due to ferrite minerals—magnetite and maghaemite—and the susceptibility frequency variation is dictated by the size and shape distribution of the magnetic domains of those ferrite minerals at sub-microscopic level [17]. It is expected that for some soils, this distribution remains identical everywhere in the soil and that only the overall concentration of ferrite changes.

When this assumption is applicable, the frequency dependence of the soil magnetic susceptibility is independent of the position, and a simpler and more efficient approach is possible. The magnetic susceptibility can be separated into a position-dependent factor and a frequency-dependent factor: $\chi(\boldsymbol{r},\omega) = \chi^{\mathrm{r}}(\boldsymbol{r})\chi^{\omega}(\omega)$. Furthermore the frequency-dependent factor can be moved out of the integral (10) to yield:

$$V^{\mathrm{t}}_{\mathrm{soil}}(t) = v_0(t)\int_{\mathcal{V}_{\mathrm{s}}} \chi^{\mathrm{r}} S \mathrm{d}V \tag{22}$$

with $V^{\mathrm{t}}_{\mathrm{soil}}(t)$ the time-domain soil response, $v_0(t) = \mathcal{F}^{-1}\{j\omega\mu_0 I^{\omega}_{\mathrm{TX}}(\omega)\chi^{\omega}(\omega)\} = \mu_0 \dfrac{\mathrm{d}I^{\mathrm{t}}_{\mathrm{TX}}(t)}{\mathrm{d}t} \otimes \chi^{\mathrm{t}}(t)$ where $\otimes$ denotes a convolution and $\chi^{\mathrm{t}}(t) = \mathcal{F}^{-1}\{\chi^{\omega}(\omega)\}$ is the normalized impulse response of the magnetic material present in the soil[6].

Expression (22) has a form similar to its frequency-domain counterpart (10). It shows that $v_0(t)$ completely defines the shape of the time domain response $V^{\mathrm{t}}_{\mathrm{soil}}(t)$, only influenced by the shape of the TX current $I^{\mathrm{t}}_{\mathrm{TX}}(t)$ and by the signature of the magnetic material $\chi^{\omega}(\omega)$ present in the soil. Hence, if χ is a separable function of space and frequency, the shape of the time domain response is independent of soil relief, concentration of magnetic material $\chi^{\mathrm{r}}(\boldsymbol{r})$, head position and orientation. Those parameters only affect the magnitude of the response.

With those numerical optimizations, the sensitivity mesh corresponding to a given head is computed in a few minutes on a standard desktop computer and the response of an arbitrary soil can then be computed in a few seconds.

[6]The unit of $\chi^{\mathrm{t}}(t)$ and $v_0(t)$ are respectively [s^{-1}] and [V/m].

V. Applications

The general model (10) allows one to efficiently compute the response of magnetic soils with low susceptibility with arbitrary relief and inhomogeneity, for an arbitrary head shape in an arbitrary position and orientation above the soil.

As this paper focuses on the model development and its validation, only simple applications are presented. In future publications, we will consider representative soil reliefs and inhomogeneities, which allows one to better understand the head behavior in real soils.

Section V-A illustrates the sensitivity maps for a double-D head configuration. To validate the two models and to assess the accuracy of their numerical implementations, Section V-B compares, for a HS configuration, the soil response obtained by the general model (10) and by the HS model (16). An additional validation is performed for the concentric head, for which an analytic solution exists. Finally, Section V-C presents the zero equi-sensitivity surface and and Section V-D presents the volume of influence; both are important characteristics of a given detector head.

A. Sensitivity maps

As an illustration of the concept of sensitivity map, Figs. 3 and 4 present vertical and horizontal cuts of the sensitivity (11) for the double-D head presented in Fig. 2 (d). For both cuts, the projections of the TX (—) and RX (– –) coils are drawn and the depths of the horizontal cuts are indicated in Fig. 3 by dot-dashed lines ($-\cdot-$). For the vertical cuts, the absolute value of the sensitivity is represented in dB to capture the large dynamic range resulting from the very fast decrease of the sensitivity with depth. For the horizontal cuts, a linear scale is used and the sensitivity is first divided by a factor α to allow a common colormap to be used for all cuts. This factor is indicated above the cut and also represented graphically by the size of the horizontal bar appearing at the top of the images.

To obtain results that are valid for any head dimensions, normalized quantities are used. Horizontal (x,y) and vertical (z) dimensions as well as the head height (h) are normalized with respect to the head characteristic length L (see Fig. 2). The normalized quantities are denoted x, y, z and h respectively. In addition, the normalized sensitivity $\mathsf{S} = SL^2$ is presented. All those normalized quantities are dimensionless and one can easily check by appropriate change of variables in the integrals (11) and (12) that S is indeed independent of the head characteristic length L. The normalized head height used is $\mathsf{h} = 0.05$.

The sensitivity map allows us to better understand how the double-D head compensates the soil response. The sensitivity is integrated over the soil volume and the negative and positive

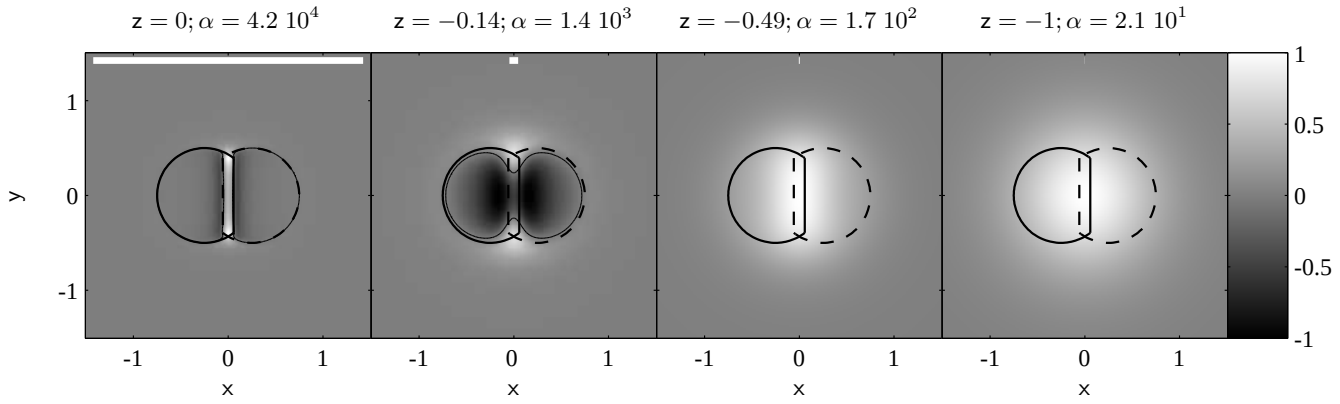

Fig. 4. Horizontal XY cuts of normalized sensitivity (S) for double-D head at $\mathsf{h} = 0.05$. Sensitivity scaling factor (α) and cut depth (z) are indicated above each cut. α is further represented by length of horizontal bar above in the image. TX (—) and RX (– –) coils as well as zero equi-sensitivity contour (—) are shown.

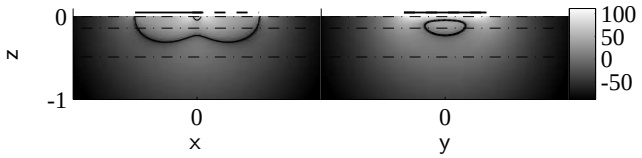

Fig. 3. Vertical XZ (left) and YZ (right) cuts of normalized absolute sensitivity ($|\mathsf{S}|$) in dB for double-D head at $\mathsf{h} = 0.05$. TX (—) and RX (– –) coils, depths of horizontal cuts (– · –) as well as zero equi-sensitivity contour (—) are shown.

parts of the volume compensate each other to produce a smaller signal in the receiver. The sensitivity is negative in a volume, shaped as two connected washbowls, close to the head and positive elsewhere. The positive and negative volumes are directly apparent in Fig. 4. On the contrary, in Fig. 3, the sign of the sensitivity is not seen directly because, in order to capture the large dynamic, the absolute value of the sensitivity is represented using a logarithm scale. However, the positive and negative volumes can be deduced from the sign reversal contour on which very strong negative values induced by the logarithmic scale appear. For clarity reasons, this contour has further been superimposed on the figures. The zero equi-sensitivity surface is also represented in Fig. 5 (b).

According to (16), the compensation of a uniform HS response is perfect if the distance between the mirrored TX coil and the RX coil is equal to the distance between the TX and RX coils[7]. This only occurs at a unique height. For other head heights, the soil response is still significantly attenuated but the compensation is not perfect. The sensitivity map also shows that the volume in which the sensitivity is negative is relatively small and exhibits high sensitivity values. Therefore, the soil properties in that volume have a strong impact on the soil response. The compensation is significantly reduced for a soil exhibiting a strong inhomogeneity or a large hole in the negative sensitivity volume.

[7]If, as we assumed, the coil overlap has been chosen to ensure a zero coupling between the coils in free space

B. HS response and implementation validation

The HS response can be computed using the general expression (10) or the simpler expression (16) valid only for a HS configuration. According to (20), $V^{\mathrm{g}}_{\mathrm{HS}}/\chi$ and $V^{\mathrm{HS}}_{\mathrm{HS}}(2+\chi)/\chi$ are independent of χ and should be equal.

Both expressions are computed using two different numerical algorithms. Indeed, according to (10), the general expression requires a volume integral on the soil volume, whereas according to (16), the HS expression requires a line integral on the RX coil. Comparing both results yields a cross-check and an indication on the accuracy of the numerical algorithms.

Furthermore, the general expression involves the magnetic fields produced by the coils while the HS expression involves the magnetic vector potential produced by the coils. Both are computed using the analytic solution for straight and circular segments. Comparing both solutions also yields a validation of the analytic expressions used and of their implementations.

To quantify the difference between the two results, the relative error $\epsilon = \left|\frac{\mathsf{V}^{\mathrm{HS}}_{\mathrm{HS}}(2+\chi)-\mathsf{V}^{\mathrm{g}}_{\mathrm{HS}}}{\mathsf{V}^{\mathrm{HS}}_{\mathrm{HS}}(2+\chi)}\right|$ is used.

It is worth emphasizing that this error, independent of χ, is used to cross-check the numerical implementations and cannot be used to assess the accuracy of the Born approximation. For this, (21), which does not require any numerical computation, should be used instead.

The χ-normalized response computed with both models, together with the corresponding error (ϵ), is presented in Table I for various heads and for a normalized head height $\mathsf{h} = 0.05$.

To avoid any dependence on the frequency, on the TX current or on the head dimension L, the dimensionless soil response $\mathsf{V}_{\mathrm{HS}} = V_{\mathrm{HS}}/(j\omega\mu_0 L I_{\mathrm{TX}})$ is used. It is easy to check by appropriate changes of variables in the integrals (10) and (12) that V_{HS} is indeed independent of the head dimension L.

The HS response is much smaller for the double-D head than for other heads, except for the quad head for which the response is null, as expected, due to the anti-symmetry of the head. As explained above, for the double-D head, the response is null only for a reference height different from the height used in Table I.

	$\frac{\mathsf{V}_{\mathrm{HS}}^{\mathrm{HS}}(2+\chi)}{\chi}$	$\frac{\mathsf{V}_{\mathrm{HS}}^{\mathrm{g}}}{\chi}$	ϵ
Circular	0.4285	0.4285	0
Concentric	0.2113	0.2112	0.0005
Elliptic	0.2716	0.2717	0.0001
Double-D	-0.0007	-0.0007	0.0035
Quad	0	0	na

TABLE I
χ-NORMALIZED DIMENSIONLESS HS RESPONSE COMPUTED WITH GENERAL ($\mathsf{V}_{\mathrm{HS}}^{\mathrm{g}}$) AND HS ($\mathsf{V}_{\mathrm{HS}}^{\mathrm{HS}}$) EXPRESSIONS TOGETHER WITH CORRESPONDING RELATIVE ERROR (ϵ) FOR NORMALIZED HEAD HEIGHT $\mathsf{h} = 0.05$.

In the case of a quad detector, the error ϵ cannot be computed because the corresponding HS response is null. For other heads, the error is quite small, which yields a good check of the numerical implementations. However, the error is the biggest for the double-D detector because the HS response is small due to a significant compensation between the positive and negative contributions in the integral (10). Such a compensation between large positive and negative contributions requires both contributions to be computed with a high accuracy in order to reach a small relative error.

For the concentric head, an additional validation has been performed by comparing $\mathsf{V}_{\mathrm{HS}}^{\mathrm{HS}}$ based on a numerical integration (17) and on the analytic solution (19) to calculate the mutual induction coefficient. The relative error was better than 10^{-15}, which provides a good validation of the implementation of (17).

C. Zero equi-sensitivity surface

As already discussed, the sign of the sensitivity can change and the volume of negative sensitivity can cause a total or partial compensation of the soil response. Therefore, visualizing the zero equi-sensitivity surface helps us to understand the compensation mechanism. This compensation is the most efficient in the case of a uniform soil and will be significantly reduced if the soil exhibits a large hole or marked inhomogeneity in the negative sensitivity volume.

For single coil heads, according to (11), the sensitivity is always positive and there is no zero equi-sensitivity surface. For the quad head, by symmetry, the zero equi-sensitivity surface is the yz plane. The zero equi-sensitivity for the other heads (concentric and double-D) are presented in Fig. 5.

For the concentric head, the zero equi-sensitivity surface looks like a circular gutter while, for the double-D head, it looks like two connected washbowls. For both heads, the negative sensitivity volume is rather small and, in that volume, the magnitude of the sensitivity is large. Therefore, holes or inhomogeneities in the negative sensitivity volume may significantly affect the soil compensation. This effect is most critical for the double-D head which exhibits a very good intrinsic compensation for homogeneous and flat soils.

D. Volume of influence

Obviously, only a limited soil volume below the head, which we call the *volume of influence*, significantly influences the soil response. The knowledge of this volume makes it possible to define objectively the sampling locations for magnetic susceptibility measurements. It also helps us to understand the detector behavior.

More specifically, the response of a uniform HS is taken as reference and the volume of influence is defined as the smallest part of that HS that produces 99% of the reference response. For this purpose, both the HS and the volume of influence are filled with a uniform soil of sufficiently weak magnetic susceptibility for the Born approximation to be valid. This definition is only valid for single coil heads because for two-coil heads, the half-space response may be null[8]. Therefore, the previous definition is further extended by considering only the volume in which the sensitivity is positive ($\mathcal{V}^+$). The volume of influence is then defined as the smallest part of $\mathcal{V}^+$ yielding 99% of the total contribution of $\mathcal{V}^+$.

In the above definition, we considered the *smallest* volume of influence. The requirement to be the smallest is mandatory to yield a unique volume. Other definitions are possible but will not be considered in this paper. It is easy to show that the *smallest* volume of influence is bound partly by an equi-sensitivity surface and partly by the horizontal plane $z = 0$. The value of the sensitivity to take into account for the equi-sensitivity surface can be found by calculating the response as a function of that sensitivity and then by finding the value for which the response is 99% of the total (positive) response.

Figure 6 shows the volume of influence for the concentric and quad heads. For the concentric head, the volume of influence is bound by an internal surface which is very similar to the zero equi-sensitivity surface presented in Fig. (5), by the horizontal plane $z = 0$ and by an oval external surface. The internal surface is an artifact resulting from our definition of the volume of influence and, in practice, the oval external surface is sufficient to characterize the volume of influence.

Furthermore, the shape of this external surface is similar for all head configurations considered with the exception of the quad head. This is due to the fact that the external surface is far away from the coils and a dipolar approximation can be used for the magnetic field emitted by the coils; the shape of the coils then becomes irrelevant. This is not true for the quad head because the dipolar moment of the RX coil is null and the quadrupole moment must be taken into account.

As the shape of the volume of influence is similar for all heads (except for the quad head), it can be efficiently characterized by the dimensionless normalized distances from the origin to the external surface along the axes: $\mathsf{R}_{\mathrm{x}}^{\mathrm{inf}} = R_{\mathrm{x}}^{\mathrm{inf}}/L$, $\mathsf{R}_{\mathrm{y}}^{\mathrm{inf}}$ and $\mathsf{R}_{\mathrm{z}}^{\mathrm{inf}}$. Those quantities are presented in Table II.

	$\mathsf{R}_{\mathrm{x}}^{\mathrm{inf}}$	$\mathsf{R}_{\mathrm{y}}^{\mathrm{inf}}$	$\mathsf{R}_{\mathrm{z}}^{\mathrm{inf}}$
Circular	1.423	1.423	1.634
Concentric	1.421	1.421	1.677
Elliptic	1.073	1.189	1.287
Double-D	2.713	2.693	3.299

TABLE II
VOLUME OF INFLUENCE CHARACTERISTICS

[8]This will be the case for any differential design such as the quad detector.

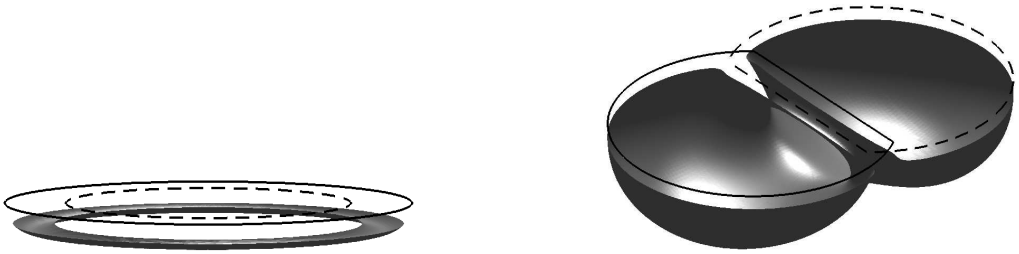

(a) (b)

Fig. 5. Zero equi-sensitivity for (a) concentric and (b) double-D head. TX (—) and RX (– –) coils are shown.

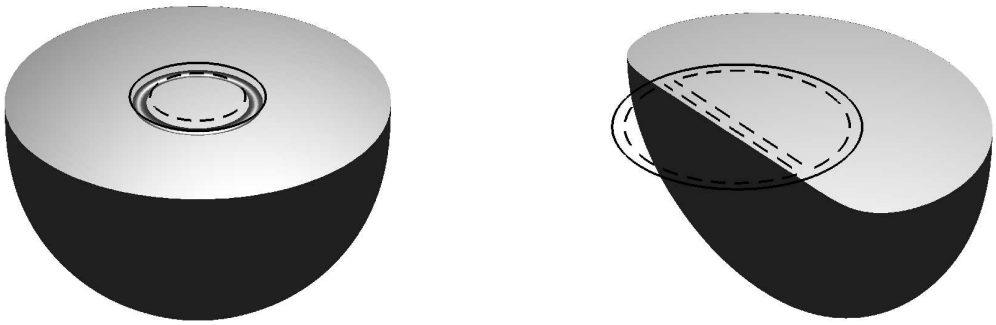

(a) (b)

Fig. 6. Volume of influence for (a) concentric and (b) quad head. TX (—) and RX (– –) coils are shown.

One can notice that the volume of influence is significantly larger for the double-D head than for other heads which indicates that for a double-D head, the soil compensation will only be efficient if the soil is homogeneous in a large volume.

VI. Conclusions and Perspectives

This paper has shown that under realistic conditions—negligible conductivity, low magnetic susceptibility—the soil response can be expressed as an integral on the soil volume of the magnetic susceptibility multiplied by the head sensitivity. Therefore, the sensitivity map helps to understand the soil response. As an illustration, the sensitivity map of a double-D head was presented and used to explain the partial soil compensation inherent to such a head design and to understand the limitations of that compensation.

This approach is both general and efficient. Indeed, when compared to available analytic solutions, it is much more general as it makes it possible to consider any coil shape and relative position, any soil inhomogeneity and relief and any head position and orientation. Further, when compared with generic numerical methods, our approach is much more efficient and makes it possible to compute the soil response for many different configurations within a reasonable time. The computation speed is further improved for heads which can be represented by line and circular segments for which the field can be calculated analytically. Additional efficiency is obtained by the introduction of dimensionless quantities which makes it possible to analyze an head design without having to specify its size. The head size only appears in the expressions relating the dimensionless quantities to their dimensional counterparts. Those expressions make it possible to assess efficiently the effect of head scaling.

In addition to the general expression, valid for any soil relief and inhomogeneity, we have also developed a simpler expression which is only valid for a homogeneous HS but which does not require the Born approximation. Comparing both approaches on a HS configuration made it possible to establish an analytic expression for the error introduced by the Born approximation as a function of the soil magnetic susceptibility. In the light of susceptibility measurements of many soils found in the literature, this expression showed that for most soils of interest within the framework of mine clearance, the corresponding error is negligible.

Comparing numerical results obtained with the two models on a HS configuration also provided a cross-check for the validity of those models and their implementations. An additional validation was obtained in the case of concentric circular loops by comparing the numerical results with the available analytic solution.

As applications of the general model, we defined the zero equi-sensitivity surface and the volume of influence which are two important characteristics of the head. Visualizing those volumes and surfaces can be very helpful in practice to understand the detector behavior. This was illustrated for representative heads designs.

As this paper focuses on the model development and validation, only simple applications have been considered. More complex scenarios including soil inhomogeneity and relief are deferred to future publications. Such scenarios are of prime interest from a practical point of view as they make it possible to compare various head designs as far as their inherent soil

compensation capabilities for realistic soils are concerned and are not limited to theoretical homogeneous and flat soils as it is often the case.

APPENDIX A
TX CURRENT IN PRESENCE OF SOIL

The TX current may be different in free space and in presence of soil. This effect is dependent on the TX coil driver circuit. For an ideal current source, the TX current is unaffected by the presence of the soil. However, for other sources, the TX current varies with the soil properties as well as with the sensor height and orientation. It is then necessary to relate the TX current in presence of soil to its free space counterpart, which can be measured and used as a detector characteristic.

In the core of the paper, we could use I_{TX} to denote the TX current without ambiguity because it was always the current in presence of soil that was meant. We will now denote the TX current in presence of soil and its free space counterpart by $I_{\mathrm{TX(as)}}$ and $I_{\mathrm{TX(fs)}}$, respectively.

To compute the TX current, let us consider that the electronics can be modeled by its Thevenin equivalent circuit composed of an ideal voltage source V_{TX} and a series impedance $Z_{\mathrm{TX}}^{\mathrm{el}}$ which can both be estimated by simple measurements on the detector. The coil can also be represented by its Thevenin equivalent circuit composed of an ideal voltage source $e_{\mathrm{TX}}^{\mathrm{soil}}$ and a series impedance $Z_{\mathrm{TX}}^{\mathrm{coil}}$. $Z_{\mathrm{TX}}^{\mathrm{coil}}$ can be estimated by simple measurements on the coil and $e_{\mathrm{TX}}^{\mathrm{soil}}$, which is the voltage induced by the soil in the TX coil[9], can be computed using (10). For this purpose, the monostatic sensitivity must be used; it can be obtained by replacing RX by TX in (11).

Note that $I_{\mathrm{TX(as)}}$, which is still to be determined, appears in (10). We therefore first compute the normalized soil response $\check{e}_{\mathrm{TX}}^{\mathrm{soil}} = e_{\mathrm{TX}}^{\mathrm{soil}}/I_{\mathrm{TX(as)}}$. We also define the total TX impedance $Z_{\mathrm{TX}} = Z_{\mathrm{TX}}^{\mathrm{el}} + Z_{\mathrm{TX}}^{\mathrm{coil}}$.

According to the Thevenin equivalent circuit, we have:

$$I_{\mathrm{TX(as)}} = \frac{V_{\mathrm{TX}} - \check{e}_{\mathrm{TX}}^{\mathrm{soil}} I_{\mathrm{TX(as)}}}{Z_{\mathrm{TX}}} \tag{A.1}$$

which immediately gives the following TX current:

$$I_{\mathrm{TX(as)}} = \frac{V_{\mathrm{TX}}}{Z_{\mathrm{TX}} + \check{e}_{\mathrm{TX}}^{\mathrm{soil}}} \tag{A.2}$$

In practice, $\check{e}_{\mathrm{TX}}^{\mathrm{soil}}$ is often much smaller than Z_{TX} and $I_{\mathrm{TX(as)}} \backsimeq I_{\mathrm{TX(fs)}} = V_{\mathrm{TX}}/Z_{\mathrm{TX}}$. In case of doubt, (A.2) can be used to check whether, for a given soil and detector, $I_{\mathrm{TX(as)}}$ can be replaced accurately by $I_{\mathrm{TX(fs)}}$ in (10) to compute the soil response.

APPENDIX B
MQS RECIPROCITY

Here, we derive the general MQS reciprocity expression. For this purpose, we consider two states defined by the magnetic permeability μ_{i}, current density $\boldsymbol{J}_{\mathrm{i}}$, magnetic field $\boldsymbol{H}_{\mathrm{i}}$ and magnetic vector potential $\boldsymbol{A}_{\mathrm{i}}$ where 'i=1,2' corresponds to the first and second states respectively. Further, the medium does not need to be homogeneous. The magnetic permeability may vary with the position and even exhibit discontinuities, typically at the interface between two media. It may also be different in the two states.

First we note that:

$$\begin{aligned}\nabla \cdot (\boldsymbol{A}_1 \times \boldsymbol{H}_2) &= \nabla \times \boldsymbol{A}_1 \cdot \boldsymbol{H}_2 - \nabla \times \boldsymbol{H}_2 \cdot \boldsymbol{A}_1 \\ &= \boldsymbol{B}_1 \cdot \boldsymbol{H}_2 - \boldsymbol{A}_1 \cdot \boldsymbol{J}_2 \end{aligned} \tag{B.1}$$

where we used the fact that, under the MQS approximation, the Ampere law becomes $\nabla \times \boldsymbol{H} = \boldsymbol{J}$.

Integrating on volume $\mathcal{V}_{\mathrm{r}}$ and applying the Gauss theorem yields:

$$\int_{\mathcal{S}_{\mathrm{r}}} (\boldsymbol{A}_1 \times \boldsymbol{H}_2) \cdot \mathrm{d}\boldsymbol{S} = \int_{\mathcal{V}_{\mathrm{r}}} (\boldsymbol{B}_1 \cdot \boldsymbol{H}_2 - \boldsymbol{A}_1 \cdot \boldsymbol{J}_2) \mathrm{d}V \tag{B.2}$$

where, according to our conventions (Section III), the surface $\mathcal{S}_{\mathrm{r}}$ is the boundary of the volume $\mathcal{V}_{\mathrm{r}}$ and the positive normal points outside.

Proceeding similarly with $\boldsymbol{A}_2 \times \boldsymbol{H}_1$ and subtracting from (B.2) yields:

$$\begin{aligned}&\int_{\mathcal{S}_{\mathrm{r}}} (\boldsymbol{A}_1 \times \boldsymbol{H}_2 - \boldsymbol{A}_2 \times \boldsymbol{H}_1) \cdot \mathrm{d}\boldsymbol{S} \\ &= \int_{\mathcal{V}_{\mathrm{r}}} \{(\mu_1 - \mu_2)\boldsymbol{H}_1 \cdot \boldsymbol{H}_2 + \boldsymbol{J}_1 \cdot \boldsymbol{A}_2 - \boldsymbol{J}_2 \cdot \boldsymbol{A}_1\} \mathrm{d}V \end{aligned} \tag{B.3}$$

which is the searched for general MQS reciprocity expression.

APPENDIX C
MUTUAL INDUCTION COEFFICIENT

Here, we relate the mutual induction coefficient between the $\widehat{\mathrm{TX}}$ coil (the mirror of the TX coil) and the RX coil to the head sensitivity.

For this purpose, we first apply reciprocity (B.3) to the HS configuration illustrated in Fig. 1 (b) in the air volume $\mathcal{V}_{\mathrm{a}}$ with the two following states:

- $\Sigma_{\widehat{\mathrm{TX}}}^{(\mathrm{fs})}$ for which the mirrored TX coil is carrying current I_{TX} in free space
- $\Sigma_{\mathrm{RX}}^{(\mathrm{fs})}$ for which the RX coil is carrying current I_{RX} in free space

This yields:

$$\begin{aligned}&\int_{\mathcal{S}_{\mathrm{as}}} \left(\boldsymbol{A}_{\widehat{\mathrm{TX}}}^{(\mathrm{fs})} \times \boldsymbol{H}_{\mathrm{RX}}^{(\mathrm{fs})} - \boldsymbol{A}_{\mathrm{RX}}^{(\mathrm{fs})} \times \boldsymbol{H}_{\widehat{\mathrm{TX}}}^{(\mathrm{fs})}\right) \cdot \mathrm{d}\boldsymbol{S} \\ &\qquad = I_{\mathrm{RX}} \int_{\mathcal{C}_{\mathrm{RX}}} \hat{\boldsymbol{l}}_{\mathrm{RX}} \cdot \boldsymbol{A}_{\widehat{\mathrm{TX}}}^{(\mathrm{fs})} \mathrm{d}l \end{aligned} \tag{C.1}$$

where $\mathcal{S}_{\mathrm{as}}$ is the air-soil interface for which the positive normal has been defined upwards. The Right-Hand Side (RHS) of the above equation was obtained from the RHS of (B.3) by noting that the first term of the volume integral is null because the permeability is the same for both states, the second term is null because in the first state ($\Sigma_{\widehat{\mathrm{TX}}}^{(\mathrm{fs})}$) there is no current in the volume considered (the upper HS) and the last term degenerates in a contour integral because the current is

[9]For a two-coil head, the Thevenin equivalent of the RX coil as well as the coupling between the TX and RX coils must be taken into account. As this generalization is straightforward, it will not be further discussed.

localized on $\mathcal{C}_{\mathrm{RX}}$. A direct application of reciprocity yields a surface integral on $\mathcal{S}_{\mathrm{air}}$ instead of $\mathcal{S}_{\mathrm{as}}$ and an opposite sign for the RHS term. The above equation can then be obtained by noting that only $\mathcal{S}_{\mathrm{as}}$ contributes to the surface integral and that the positive normal of $\mathcal{S}_{\mathrm{as}}$ and $\mathcal{S}_{\mathrm{air}}$ are in opposite directions on that surface.

By symmetry, the currents, fields and potentials of the mirrored coil are related to the original one as follows:

$$\begin{aligned}\boldsymbol{J}_{\widehat{\mathrm{TX}}}(x,y,z) &= \pm\boldsymbol{J}_{\mathrm{TX}}(x,y,-z)\\ \boldsymbol{A}_{\widehat{\mathrm{TX}}}(x,y,z) &= \pm\boldsymbol{A}_{\mathrm{TX}}(x,y,-z)\\ \boldsymbol{H}_{\widehat{\mathrm{TX}}}(x,y,z) &= \mp\boldsymbol{H}_{\mathrm{TX}}(x,y,-z)\end{aligned} \tag{C.2}$$

where the upper sign is valid for x and y coordinates and the lower sign is valid for the z coordinate.

Therefore, on $\mathcal{S}_{\mathrm{as}}$ where $z=0$ and $\hat{\boldsymbol{n}}=\hat{\boldsymbol{z}}$, $\boldsymbol{A}^{(\mathrm{fs})}_{\widehat{\mathrm{TX}}}\times\hat{\boldsymbol{n}} = \boldsymbol{A}^{(\mathrm{fs})}_{\mathrm{TX}}\times\hat{\boldsymbol{n}}$ and $\boldsymbol{H}^{(\mathrm{fs})}_{\widehat{\mathrm{TX}}}\times\hat{\boldsymbol{n}} = -\boldsymbol{H}^{(\mathrm{fs})}_{\mathrm{TX}}\times\hat{\boldsymbol{n}}$ and (C.1) becomes:

$$\int_{\mathcal{S}_{\mathrm{as}}}\left(\boldsymbol{A}^{(\mathrm{fs})}_{\mathrm{TX}}\times\boldsymbol{H}^{(\mathrm{fs})}_{\mathrm{RX}}+\boldsymbol{A}^{(\mathrm{fs})}_{\mathrm{RX}}\times\boldsymbol{H}^{(\mathrm{fs})}_{\mathrm{TX}}\right)\cdot\mathrm{d}\boldsymbol{S} = I_{\mathrm{RX}}\int_{\mathcal{C}_{\mathrm{RX}}}\boldsymbol{A}^{(\mathrm{fs})}_{\widehat{\mathrm{TX}}}\cdot\mathrm{d}\boldsymbol{l} \tag{C.3}$$

The first term of the Left-Hand Side (LHS) can be further developed by applying again reciprocity in the soil volume $\mathcal{V}_{\mathrm{soil}}$ between the following states:

- $\Sigma^{(\mathrm{fs})}_{\mathrm{TX}}$ for which the TX coil is carrying a current I_{TX} and is in free space and
- $\Sigma^{(0)}_{\mathrm{RX}}$ for which the RX coil is carrying a current I_{RX} in a fictitious medium for which $\mu=0$. For that medium, $\boldsymbol{H}^{(0)}_{\mathrm{RX}}=\boldsymbol{H}^{(\mathrm{fs})}_{\mathrm{RX}}$ and $\boldsymbol{A}^{(0)}_{\mathrm{RX}}=0$.

This yields

$$\int_{\mathcal{S}_{\mathrm{as}}}\boldsymbol{A}^{(\mathrm{fs})}_{\mathrm{TX}}\times\boldsymbol{H}^{(\mathrm{fs})}_{\mathrm{RX}}\cdot\mathrm{d}\boldsymbol{S}=\mu_0\int_{\mathcal{V}_{\mathrm{soil}}}\boldsymbol{H}^{(\mathrm{fs})}_{\mathrm{TX}}\cdot\boldsymbol{H}^{(\mathrm{fs})}_{\mathrm{RX}}\mathrm{d}V \tag{C.4}$$

where we used the fact that only $\mathcal{S}_{\mathrm{as}}$ contributes to the surface integral on $\mathcal{S}_{\mathrm{soil}}$ and that the positive normal of $\mathcal{S}_{\mathrm{as}}$ and $\mathcal{S}_{\mathrm{soil}}$ are identical on that surface.

The second term of the LHS of (C.3) can be obtained as the first one by interchanging 'RX' and 'TX'. Therefore, according to (C.4), both terms are equal. According to (17), the RHS of (C.3) is equal to $I_{\mathrm{TX}}I_{\mathrm{RX}}M_{\widehat{\mathrm{TX}},\mathrm{RX}}$ where $M_{\widehat{\mathrm{TX}},\mathrm{RX}}$ is the mutual induction coefficient between the mirrored TX coil and the RX coil.

One finally gets the following expression for the mutual induction coefficient:

$$M_{\widehat{\mathrm{TX}},\mathrm{RX}}=2\mu_0\int_{\mathcal{V}_{\mathrm{s}}}S\mathrm{d}V \tag{C.5}$$

with S defined in (11).

ACKNOWLEDGMENT

The authors wish to thank I. van den Bosch for his useful comments and suggestions.

REFERENCES

[1] Y. Das, J. McFee, and R. H. Chesney, "Time domain response of a sphere in the field of a coil: Theory and experiment." *IEEE transactions on geoscience and remote sensing.*, vol. GE-22, no. 4, pp. 360–367, July 1984.

[2] Y. Das, J. McFee, J. Toews, and G. Stuart, "Analysis of an electromagnetic induction detector for real-time location of buried objects." *IEEE transactions on geoscience and remote sensing.*, vol. 28, no. 3, pp. 278–288, May 1990.

[3] Y. Das and J. McFee, "A simple analysis of the electromagnetic response of buriedconducting objects." *IEEE transactions on geoscience and remote sensing.*, vol. 29, no. 2, pp. 342–344, March 1991.

[4] T. Grzegorczyk, B. Zhang, J. A. Kong, B. Barrowes, and K. O'Neill, "Electromagnetic induction from highly permeable and conductive ellipsoids under arbitrary excitation: application to the detection of unexploded ordnances." *IEEE transactions on geoscience and remote sensing.*, vol. 46, no. 4, pp. 1164–1176, April 2008.

[5] P. P. Silvester and D. Omeragic, "Sensitivity of metal detectors to spheroidal targets." *IEEE transactions on geoscience and remote sensing.*, vol. 33, no. 6, pp. 1331–1335, November 1995.

[6] F. Shubitidze, K. O'Neill, I. Shamatava, K. Sun, and K. Paulsen, "Fast and accurate calculation of physically complete EMI response by a heterogeneous metallic object." *IEEE transactions on geoscience and remote sensing.*, vol. 43, no. 8, pp. 1736–1750, August 2005.

[7] J. L. Stalnaker, M. E. Everett, A. Benavides, and C. J. Pierce, "Mutual induction and the effect of host conductivity on the em induction response of buried plate targets using 3-d finite-element analysis." *IEEE transactions on geoscience and remote sensing.*, vol. 44, no. 2, pp. 251–259, February 2006.

[8] N. Geng, C. Baum, and L. Carin, "On the low-frequency natural response of conducting and permeable targets." *IEEE transactions on geoscience and remote sensing.*, vol. 37, no. 1, pp. 347–359, January 1999.

[9] C. Gaudin, C. Sigrist, and C. Bruschini, "Metal detectors for humanitarian demining: a patent search and analysis," Vrije Universiteit Brussel, Brussels, Belgium," EUDEM2 Technology Survey Report, November 2003. [Online]. Available: http://www.eudem.info/

[10] Y. Das, "A preliminary investigation of the effects of soil electromagnetic properties on metal detectors," in *Proc. SPIE Conference on Detection and Remediation Technologies for Mines and Mine-like Targets IX, 5415*, Orlando, FL, USA, April 2004, pp. 677–690.

[11] ——, "Electromagnetic induction response of a target buried in conductive and magnetic soil." in *Proc. SPIE Conference on Detection and Remediation Technologies for Mines and Mine-like Targets X, 5794*, Orlando, FL, USA, June 2005, pp. 263–274.

[12] ——, "Effects of soil electromagnetic properties on metal detectors." *IEEE Transaction on Geoscience and Remote Sensing*, vol. 44, no. 6, pp. 1444–1453, June 2006.

[13] ——, "Time-domain response of a metal detector to a target buried in soil with frequency-dependent magnetic susceptibility." in *Proc. SPIE Conference on Detection and Remediation Technologies for Mines and Mine-like Targets XI, 6217*, Orlando, FL, USA, April 2006.

[14] P. Druyts, Y. Das, C. Craeye, and M. Acheroy, "Effect of the soil on the metal detector signature of a buried mine," in *Proc. SPIE Defence and Security Symposium*, Orlando, FL, USA, April 2006.

[15] C. Bruschini, "On the low frequency EMI response of coincident loops over a conductive and permeable soil and corresponding background reduction schemes," *IEEE Transaction on Geoscience and Remote Sensing*, vol. 42, no. 8, pp. 1706–1719, Augutsus 2004.

[16] T. Lee and R. Lewis, "Transient EM response of a large loop on a layered ground." *Geophysical Prospecting*, vol. 22, no. 3, pp. 430–444, September 1974.

[17] S. D. Billings, L. R. Pasion, D. W. Oldenburg, and J. Foley, "The influence of magnetic viscosity on electromagnetic sensors," in *EUDEM-SCOT2 2003, International Conference on Requirements and Technologies for the Detection, Removal and Neutralization of Landmines and UXO*, Brussels, Belgium, September 2003.

[18] J. R. Wait and R. H. Ott, "On calculating transient electromagnetic fields of a small current-carrying loop over a homogeneous earth," *Pure and Applied Geophysics*, vol. 95, no. 1, pp. 157–162, December 1972.

[19] C. Moreland., "Coil basics," Geotech, Tech. Rep., 2006. [Online]. Available: http://geotech.thunting.com/pages/metdet/info/coils.pdf

[20] D. Guelle, M. Gaal, M. Bertovic, C. Mueller, M. Scharmach, and M. Pavlovic, "South-east europe interim report field trial croatia (continuation of the ITEP-project systematic test and evaluation of metal detectors - STEMD) 25 september 18 october 2006," BAM,

Bundesanstalt fr Materialforschung und prfung, Tech. Rep., March 2007. [Online]. Available: http://www.itep.ws/
[21] A. M. Lewis, T. J. Bloodworth, D. M. Guelle, F. R. Littmann, A. Logreco, and M. A. Pike, "Systematic test and evaluation of metal detectors (STEMD) — interim report laboratory tests italy." JRC, Joint Research Centre of the European Commission, Tech. Rep. EUR22536EN, December 2006. [Online]. Available: http://www.itep.ws/
[22] D. M. Guelle, A. M. Lewis, M. A. Pike, A. Carruthers, and S. M. Bowen, "Systematic test and evaluation of metal detectors (STEMD). interim report field trial lao, 27 september–5 november 2004," JRC, Joint Research Centre of the European Commission, Tech. Rep. S.P.I05.24, March 2005. [Online]. Available: http://www.itep.ws/
[23] D. M. Guelle, A. M. Lewis, M. A. Pike, and C. Craill, "Systematic test and evaluation of metal detectors (STEMD). interim report field trial mozambique, 12 april–5 may 2005." JRC, Joint Research Centre of the European Commission, Tech. Rep. EUR21886EN, November 2005. [Online]. Available: http://www.itep.ws/
[24] R. V. Dam, J. Hendrickx, J. Harrison, B. Borchers, D. I. Norman, S. Ndur, C. Jasper, P. Niemeyer, R. Nartey, D. Vega, L. Calvo, and J. E. Simms, "Spatial variability of magnetic soil properties." in *Detection and Remediation Technologies for Mines and Minelike Targets IX, 5415*, Orlando, FL, USA, 2004, pp. 665–676.
[25] R. V. Dam, J. Harrison, J. Hendrickx, D. Hirschfeld, R. North, J. S. Y., and Li, "Mineralogy of magnetic soils at a UXO remediation site in kaho'olawe hawaii." in *18th Annual Symposium on the Application of Geophysics to Engineering and Environmental Problems.*, Atlanta, USA, April 2005.
[26] R. V. Dam, J. Hendrickx, J. Harrison, and B. Borchers, "Conceptual model for prediction of magnetic properties in tropical soils." in *Detection and Remediation Technologies for Mines and Minelike Targets X, 5794*, Orlando, FL, USA, 2005, pp. 177–187.
[27] Herman A. Haus and James R. Melcher, *Electromagnetic Fields and Energy*. MIT Hypermedia Teaching Facility, 1998. [Online]. Available: http://web.mit.edu/6.013_book/www/index.html
[28] A. F. Peterson, S. L. Ray, and R. Mittra, *Computational Methods for Electromagnetics*, ser. IEEE/OUP Series on Electromagnetic Wave Theory. New York: IEEE Press, 1998.
[29] J. Stratton, *Electromagnetic theory*, I. S. in Physics, Ed. McGraw-Hill Book Company, 1941.
[30] R. F. Harrington, *Time-Harmonic Electromagnetic Fields*. Wiley-IEEE Press, 2001.
[31] J. van der Kruk, E. Slob, J. Fokkema, and P. van den Berg, "General framework for describing electrical and electromagnetic exploration methods." in *Expanded Abstracts with Author's Biographies Volume 1, Society of Exploration Geophyisicists International Exposition and Sixty-Seventh Annual Meeting*, Dallas, Texas, USA, November 1997, pp. 374–377.
[32] J. van der Kruk, "Three-dimensional imaging of multicomponent ground-penetrating radar data," Master's thesis, Delft University of Technology, Delft, The Netherlands, 2001.
[33] B. A. Auld and J. C. Moulder, "Review of advances in quantitative eddy current nondestructive evaluation." *Journal of Nondestructive Evaluation.*, vol. 18, no. 1, pp. 3–36, March 1999.
[34] C. E. Baum, *Detection and Identification of Visually Obscured Targets*, C. E. Baum, Ed. Taylor and Francis, 1998.
[35] W. C. Chew, *Waves and Fields in Inhomogeneous Media*. Van Nostrand Reinhold, 1990.
[36] S. F. Gruber and J. D. Norgard, "Dielectric oblate spheroidal model of buried landmines." in *Proc. SPIE Conference on Detection and Remediation Technologies for Mines and Mine-like Targets VI, 4394*, Orlando, FL, USA, April 2001, pp. 1316–1324.
[37] P. P. Silvester and D. Omeragic, "Sensitivity maps for metal detector design." *IEEE transactions on geoscience and remote sensing.*, vol. 34, no. 3, pp. 788–792, May 1996.
[38] L. K. Urankar, "Vector potential and magnetic field of current-carrying finite arc segment in analytic form, part I: Filament approximation." *IEEE Transactions on magnetics*, vol. 16, no. 5, pp. 1283–1288, September 1980.
[39] CEN workshop 7, "CEN workshop agreement, humanitarian and evaluation, metal detectors," CEN, European Committee for Standardization, Tech. Rep. CWA14747:2003, June 2003.

Pascal Druyts received the M.Sc. degree in electrical engineering in 1991 and the postgraduate degree in automatic control in 1992, both from the Université Libre de Bruxelles, Brussels, Belgium. Since 1992, he is with the Signal and Image Centre of the Royal Military Academy in Brussels. His current research is on the modeling of EMI sensors and ground penetrating radars within the framework of mine clearance.

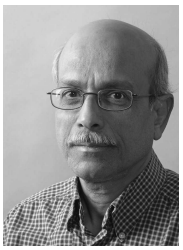

Yogadhish Das received the Bachelors degree in electronics and electrical communication engineering from the Indian Institute of Technology, Kharagpur,in 1970, the Masters degree from the University of New Brunswick in 1972 and the Ph.D. degree from the University of Manitoba, Winnipeg, MN, Canada in 1977, both in electrical engineering. He has been with the Threat Detection Group, Defence R&D Canada – Suffield since 1977, where most of his work has been in Unexploded Ordnance and landmine detection for military countermine as well as humanitarian demining. His current research interest is in understanding the effect of soil on landmine detection devices. He has been a member of the Institute of Electrical and Electronics Engineers since 1977 and was elected a Fellow in 2000 "for contributions and leadership in electrical techniques of location and identification of buried objects".

Christophe Craeye was born in Belgium in 1971. He received the M.S. degree in electrical engineering and the Ph.D. He received the Electrical Engineer and Bachelier in Philosophy degrees in 1994, and the Ph.D. degree in Applied Sciences in 1998, all from the Université catholique de Louvain (UCL). From 1994 to 1999, he was a teaching assistant at UCL and carried out research on the radar signature of the sea surface perturbed by rain, in collaboration with the Rain-sea interaction facility of NASA, Wallops Island (VA) and with the European Space Agency. From 1999 to 2001, he stayed as a post-doc researcher at the Eindhoven University of Technology, at the Netherlands Institute for Research in Astronomy and at the University of Massachusetts. His post-doctoral research concerned wideband array analysis, in the framework of the Square Kilometer Array radio telescope project. Since 2002, he is an Associate Professor at the Université catholique de Louvain. His research interests are finite antenna arrays, multiple antenna systems, numerical methods for fields in periodic media, small antennas and microwave detection. He participates to the COST IC0603 Action on Antennas for Sensor applications. He currently is an Associate Editor of the IEEE Transactions on Antennas and Propagation.

Marc Acheroy received the engineering degree in mechanics from the Royal Military Academy (RMA), Brussels, Belgium, in 1971, the engineering degree in control and automation in 1981 and the Ph.D. degree in applied sciences in 1983, both from the Université Libre de Bruxelles, Brussels, Belgium. He is now a Professor in signal processing and automatic control in the polytechnic Faculty of the RMA and the Head of the Communication, Information, Signal and Sensor Department of the RMA. He has a solid expertise in image restoration and compression, in pattern recognition, data fusion and mine action technologies. He is leading several projects, among which projects for the Defence, the European Commission, the European Space Agency and the Belgian scientific Policy.